

Discovery and Characterization of a Substrate Selective p38 α Inhibitor

Walter Davidson,[‡] Lee Frego,[‡] Gregory W. Peet, Rachel R. Kroe, Mark E. Labadia, Susan M. Lukas, Roger J. Snow, Scott Jakes, Christine A. Grygon, Christopher Pargellis, and Brian G. Werneburg*

Department of Immunology and Inflammation, Boehringer Ingelheim Pharmaceuticals, Research and Development Center, 900 Ridgebury Road, Ridgefield, Connecticut 06877

Received March 11, 2004; Revised Manuscript Received June 14, 2004

ABSTRACT: A novel inhibitor of p38 mitogen-activated protein kinase (p38), CMPD1, identified by high-throughput screening, is characterized herein. Unlike the p38 inhibitors described previously, this inhibitor is substrate selective and noncompetitive with ATP. In steady-state kinetics experiments, CMPD1 was observed to prevent the p38 α -dependent phosphorylation ($K_i^{\text{app}} = 330$ nM) of the splice variant of mitogen-activated protein kinase-activated protein kinase 2 (MK2a) that contains a docking domain for p38 α and p38 β , but it did not prevent the phosphorylation of ATF-2 ($K_i^{\text{app}} > 20$ μ M). In addition to kinetic studies, isothermal titration calorimetry and surface plasmon resonance experiments were performed to elucidate the mechanism of inhibition. While isothermal titration calorimetry analysis indicated that CMPD1 binds to p38 α , CMPD1 was not observed to compete with ATP for p38 α , nor was it able to interrupt the binding of p38 α to MK2a observed by surface plasmon resonance. Therefore, deuterium exchange mass spectrometry (DXMS) was employed to study the p38 α ·CMPD1 inhibitory complex, to provide new insight into the mechanism of substrate selective inhibition. The DXMS data obtained for the p38 α ·CMPD1 complex were compared to the data obtained for the p38 α ·MK2a complex and a p38 α ·active site binding inhibitor complex. Alterations in the DXMS behavior of both p38 α and MK2a were observed upon complex formation, including but not limited to the interaction between the carboxy-terminal docking domain of MK2a and its binding groove on p38 α . Alterations in the D₂O exchange of p38 α produced by CMPD1 suggest that the substrate selective inhibitor binds in the vicinity of the active site of p38 α , resulting in perturbations to regions containing nucleotide binding pocket residues, docking groove residues (E160 and D161), and a Mg²⁺ ion cofactor binding residue (D168). Although the exact mechanism of substrate selective inhibition by this novel inhibitor has not yet been disclosed, the results suggest that CMPD1 binding in the active site region of p38 α induces perturbations that may result in the suboptimal positioning of substrates and cofactors in the transition state, resulting in selective inhibition of p38 α activity.

Signal transduction through the p38¹ pathway is required for the production of inflammatory cytokines, such as TNF α

* To whom correspondence should be addressed. Telephone: (203) 798-5518. Fax: (203) 791-6196. E-mail: bwernebu@rdg.boehringer-ingelheim.com.

[‡] These authors contributed equally to this work.

¹ Abbreviations: ATF-2, activating transcription factor 2; BSA, bovine serum albumin; CDX3, caudal-type homeo box transcription factor 3; CHAPS, 3-[(3-cholamidopropyl)dimethylammonio]-1-propanesulfonate; CHOP, C/EBP homologous protein 10; CMPD, compound; DMSO, dimethyl sulfoxide; DXMS, deuterium exchange mass spectrometry; ESI, electrospray ionization; FTMS, Fourier transform mass spectrometry; fwhm, full width at half-maximum; GADD135, growth arrest DNA damage 135; GSH, glutathione; GST, glutathione S-transferase; HEPES, 4-(2-hydroxyethyl)-1-piperazineethanesulfonic acid; IFN γ , interferon γ ; IL-1, interleukin 1; IL-6, interleukin 6; ITC, isothermal titration calorimetry; LSP1, lymphocyte specific protein 1; MEF, myocyte enhancing factor; MK, mitogen-activated protein kinase-activated protein kinase; MKK, mitogen-activated protein kinase kinase; MNK, mitogen-activated protein kinase-interacting serine/threonine kinase 1; MSK, mitogen and stress response kinase 1; NFAT, nuclear factor of activated T-cells; NES, nuclear export signal; NLS, nuclear localization signal; p38, p38 mitogen-activated protein kinase; SAP, stress-activated protein; SPR, surface plasmon resonance; STAT1, signal transducer and activator of transcription 1; TCEP, tris(2-carboxyethyl)-phosphine hydrochloride; TES, N-tris(hydroxymethyl)methyl-2-aminoethanesulfonic acid; TNF α , tumor necrosis factor α .

and IL-1 β , which propagate inflammation in autoimmune disorders (1–4). Biological therapies directed against these inflammatory cytokines, anti-TNF α (5, 6) and anti-IL-1 β , are effective for ameliorating the symptoms of chronic inflammation. As a consequence, the development of an effective, economical, and orally available small molecule alternative for autoimmune disease therapy that targets the p38 pathway is a goal of pharmaceutical research.

The prototypical p38 pathway inhibitor, SB203580 (7), is an ATP competitive pyridinylimidazole inhibitor of p38 α and p38 β that inhibits signal transduction downstream of p38, leading to a reduction in the level of TNF α production in cell culture. Recently, the ATP competitive p38 α inhibitor, BIRB 796, a diarylurea compound with slow-tight binding characteristics and improved specificity, has been shown to abrogate TNF α production in cell culture at low nanomolar concentrations (8). BIRB 796 utilizes a novel allosteric binding pocket that results from a conformational change in p38 α induced by inhibitor binding. Early analogues of BIRB 796 (8) bound proximal to the ATP pocket, with no direct overlap. A conformational change in the DFG loop of the active site produces a structure incompatible with ATP

binding; therefore, this class of compounds precludes the phosphorylation of all p38 α substrates.

The p38 pathway mediates multiple cellular functions in addition to the propagation of inflammation, including migration (9, 10), survival (11), and cell death (12). To accomplish its many functions, p38 phosphorylates several transcription factors, including MEF2A, MEFC, SAP1, CHOP, GADD135, STAT1, NFAT, CDX3, and ATF-2, and it activates several downstream kinases via phosphorylation, including MSK1/2, MNK1, MK2, MK3, and MK5 (13). p38 α has been shown to contain a binding groove capable of recognizing docking sites present on both upstream kinase activators and downstream substrates, including MEF2A, MEF2C, MKK3b, MKK6, and the MKs.

Site-directed mutagenesis studies have demonstrated that two moieties of the p38 α docking groove are important for binding. The CD domain, composed of residues D313, D315, and D316 (14), and the ED domain, comprising residues E160 and D161 (15), affect interactions with activators and substrates. Mutations in these acidic patches at both ends of the p38 α docking groove result in reduced levels of phosphorylation of the MKs. Specific mutations of the ED domain have been observed to confer substrate (MK3) selective inhibition of p38 activity (15).

Structures of unphosphorylated p38 α have been determined by X-ray crystallographic analysis (16, 17). X-ray crystallographic analysis of the p38 α binary complexes, containing the docking site peptides of MEF2A and MKK3b, identified additional residues, I116 and Q120, of the docking groove involved in binding (18). Conformational changes local to the binding groove and specific conformational changes in the active site of p38 α have been observed upon binding of the MEF2A and MKK3b docking peptides. Thus, the interactions mediated by the p38 docking groove appear to be critical for specific complex formation and signal transduction required for multiple cellular functions. The inhibition of specific p38 signaling complexes could be an effective method for selectively blocking undesirable functions of the p38 pathway, such as the chronic production of inflammatory cytokines.

One of the p38 α and p38 β substrates, MK2, is required for the production of maximal levels of TNF α , IL-1 β , IL-6, and IFN γ (19). We have discovered that the MK2a splice variant of MK2, which contains a docking domain for both p38 α and p38 β , forms a high-affinity complex with p38 α (20). Binding energy contributed by the interaction between the 30-amino acid carboxy-terminal docking domain of MK2a and the p38 α docking groove is required for efficient MK2a activation. This tight interaction, the strongest yet encountered between p38 α and a signaling partner, is essential for p38 α pathway signal transduction through MK2 in cells (19, 21). The p38 α -MK2a complexes are required for efficient activation of MK2a, nucleocytoplasmic transport of active p38 α and MK2a, and post-transcriptional regulation of TNF α (22–26). Inhibition of MK2a phosphorylation by p38 α is a plausible mechanism for specifically blocking the post-transcriptional regulation of TNF α production by p38 signal transduction.

This report describes the discovery of a p38 α inhibitor that is noncompetitive with ATP and specifically blocks the activation of MK2a by p38 α *in vitro*. The compound described herein does not prevent the phosphorylation of

ATF-2 under the conditions that were tested, and it does not prevent formation of the p38 α -MK2a complex. To gain a better understanding of the mechanism of substrate selective inhibition, a novel application of deuterium exchange mass spectrometry (DXMS) was utilized to study the binding interactions between p38 α and three binding partners: MK2a, an active site binding inhibitor similar to BIRB 796 (CMPD2), and an MK2a specific p38 α inhibitor (CMPD1).

DXMS is a powerful technique for the study of protein structure, protein–protein interactions, and protein–ligand interactions (27–34). This technique measures the extent of exchange between backbone amide hydrogens and deuterated water via subsequent peptic digestion and rapid high-performance liquid chromatography–mass spectrometry. The digestion produces peptides whose extent of exchange at several time points is monitored by mass spectrometry. The resolution of the technique is limited by the length of the peptides produced in the digestion. DXMS measurements report chemical environment and secondary structure. The exchange rates are altered by hydrogen bonding, burial within the protein structure, formation of the protein–protein complex, or formation of the protein–ligand complex. In this work, alterations in exchange for both p38 α and MK2a upon complex formation are studied, and these results are discussed in relation to alterations in p38 α DXMS produced by binding with the MK2a selective inhibitor of p38 α (CMPD1). The DXMS experiments have improved our understanding of the interactions between p38 α , MK2a, and the substrate selective p38 α inhibitor. The results indicate that CMPD1 binds in the vicinity of the active site, causing local perturbations to regions containing docking groove residues, nucleotide binding pocket residues, and residues involved in binding a metal ion cofactor.

EXPERIMENTAL PROCEDURES

Expression and Purification of Signaling Reagents. The cDNA encoding murine p38 α was cloned into pET15b (Novagen), expressed in bacteria with a 5His affinity tag at the amino terminus, and purified to greater than 95% purity, as described previously (35). Purified p38 α was dually phosphorylated at residues T180 and Y182, as described previously (20). Downstream substrates, including 6His–MK2a 51–400, GST–MK2a 1–400, and GST–ATF-2 1–109, were expressed and purified as described previously (20).

Steady-State Kinetics Assays. The phosphorylation of 6His–MK2a 51–400 and GST–ATF-2, catalyzed by activated p38 α , was assessed in 20 mM HEPES (pH 7.6), 50 mM KCl, 10 mM MgCl₂, 100 μ M Na₃VO₄, 0.01% CHAPS, 1 mM DTT, 10 μ g/mL bovine serum albumin, and [γ -³³P]-ATP (500–1500 Ci/mol). The enzyme was activated by dual phosphorylation of the TGY sequence (74% as determined by mass spectrometry). The phosphorylation of MK2a and ATF-2 constructs by catalytic amounts of activated p38 α was quenched with 10% trichloroacetic acid and 5 mM inorganic pyrophosphate. Phosphorylated MK2a and ATF-2 products were captured with filter plates followed by scintillation counting to determine the moles of product formed. The velocity of product formation was determined by linear regression. The inhibition of p38 α catalysis of MK2a and ATF-2 phosphorylation was assessed in the

presence of CMPD1. The inhibitor and substrate (ATP) concentrations were varied to determine the potency and the mechanism of inhibition. The reciprocal velocity was plotted against the reciprocal ATP concentration, and the data were fit by linear regression to generate a Lineweaver–Burk plot. The velocities were also plotted versus the ATP concentration, and the data were fit globally to ATP noncompetitive inhibition models with Enzyme Kinetics Module 1.1 of Sigma Plot 8. The noncompetitive partial mechanism is one in which the noncompetitive inhibitor reduces the enzyme-catalyzed rate of product formation by a factor of β : $v = V_{\max}/[(1 + K_M/[S])(1 + [I]/K_i)/(1 + [I]\beta/K_i)]$. The mixed partial mechanism is one in which the noncompetitive inhibitor reduces the enzyme-catalyzed rate of product formation by a factor of β , and decreases the affinity of the substrate for the enzyme by a factor of α : $v = V_{\max}\{[1 + \beta[I]/(\alpha K_i)]/[1 + [I]/(\alpha K_i)]\}/\{1 + (K_M/[S])(1 + [I]/K_i)/[1 + [I]/(\alpha K_i)]\}$.

Isothermal Titration Calorimetry. The isothermal titration calorimetry experiments were performed using a Microcal (Northampton, MA) VP-ITC. To measure the extent of binding to p38 α , the sample cell of the calorimeter was loaded with 30 μ M test compound in 20 mM TES (pH 7.0), 200 mM NaCl, 1 mM TCEP, and 1% DMSO. The syringe was loaded with 250 μ M p38 α in the same buffer. To measure the level of binding to GST–MK2a 1–400, the sample cell was loaded with 30 μ M test compound in 20 mM TES (pH 7.0), 200 mM NaCl, 1 mM TCEP, and 1% DMSO. The syringe was loaded with 206 μ M GST–MK2a 1–400. The solubility of the test compounds dictated whether the protein was loaded into the sample cell or the syringe. All solutions were degassed for 8 min, and titrations were performed at 25 °C. After completion of the titration, baselines were manually drawn and subtracted from the data. For the GST–MK2a 1–400 binding experiments, the data were zeroed using control titrations of protein into buffer. For the p38 α experiments, the data were zeroed assuming that the final injections of each titration represent only the heat of dilution. The data were fit using a one-site binding model available in the Origin ITC data analysis software (version 5.0).

Surface Plasmon Resonance. SPR experiments were performed on a BIAcore 3000 (BIAcore, Inc.). Anti-GST antibody (BIAcore, Inc.), at a concentration of 20 μ g/mL in 10 mM sodium acetate (pH 5.0), was immobilized to 3000 resonance units on a BIAcore CM4 chip using the standard amine coupling protocol. GST–MK2a 1–400 was injected over the anti-GST surface at a concentration of 500 nM in a buffer consisting of 50 mM Tris–HCl (pH 8.0), 100 mM NaCl, 0.01% BSA, 0.01% CHAPS, and 500 μ M TCEP. GST–MK2a 1–400 was injected over the anti-GST surface until a density of 500–1000 resonance units was reached.

All solution competition experiments were carried out at 25 °C in an assay buffer consisting of 50 mM Tris–HCl (pH 8.0), 100 mM NaCl, 0.01% BSA, 0.01% CHAPS, 500 μ M TCEP, and 1% DMSO. The test compound and p38 α were diluted to 1 μ M and 5 nM, respectively, in buffer containing 1% DMSO. The p38 α /compound mixture was then injected over the GST–MK2a 1–400 surface at a flow rate of 30 μ L/min, and equilibrium data were collected.

Fluorescence Binding Experiments. CMPD2 (35) and CMPD3 (8) are slow-tight binding analogues of BIRB 796;

CMPD3 displays enhanced fluorescence upon binding to p38 α . The change in fluorescence (excitation λ = 330 nm; emission λ = 384 nm) upon binding of CMPD3 to p38 α and activated p38 α was measured in 20 mM Bis-Tris-propane (pH 7.0), 2 mM EDTA, 0.01% NaN₃, 0.15% *n*-octyl glucoside, and 2% DMSO. The concentrations of p38 α and CMPD3 used in the experiment were 170 and 500 nM, respectively. To test for competition between CMPD1 and CMPD3, the change in fluorescence upon binding of CMPD3 to p38 α and activated p38 α (63% dual phosphorylation of the TGY sequence as determined by mass spectrometry) was repeated in the presence of 5 μ M CMPD1. An inner filter effect was not observed in the presence of 5 μ M CMPD1. The experiments were performed with an SLM Aminco Bowman Series 2 Model SQ-340 fluorescence spectrophotometer.

Thermal Denaturation Assay. A UV thermal melt experiment with p38 α and CMPD3 was carried out using a Perkin-Elmer Lambda 40 spectrophotometer. For each measurement, a quartz cuvette was loaded with 2.5 μ M p38 α and 25 μ M inhibitor in 10 mM sodium phosphate (pH 7.0), 100 mM NaCl, and 1 mM TCEP (a reducing agent). Absorbance data at 230 nm were collected as the temperature was scanned from 25 to 80 °C at a ramp rate of 0.2 °C/min. The melting temperature for each sample was calculated as the maximum deflection point of the first derivative of the melting transition using the Perkin-Elmer Templab software (version 1.62). The T_m values are converted into K_a values using the equation $T_m = 3.08(\log K_a) + 31.2$. A detailed description of this method has been reported previously (35).

Identification of Peptides in Deuterium Exchange Experiments. Peptides generated from each protein (MK2a and p38 α) by peptic digestion were identified. Pepsin cleavage is reproducible but difficult to predict. The protein was digested with pepsin for 5 min at 0 °C. The resulting peptides were subjected to μ HPLC/FTMS analysis. Mobile phase A consisted of 98.9% water, 1% acetonitrile, and 0.1% formic acid; mobile phase B consisted of 5% water, 95% acetonitrile, and 0.1% formic acid. The flow rate was 5 μ L/min, with a 10 μ L injection onto a 150 mm \times 0.3 mm PepMap C18 column (LC Packings, San Francisco, CA). The gradient program was from 0 to 100% B at 38 min, held until 54 min. FTMS spectra (Bruker ApexII, Billerica, MA) were acquired from m/z 400 to 1800. Seven 1.5 s spectra were accumulated for each stored spectrum with a length of 256K, and a resolution of 50 000. External calibration was performed by in-source fragmentation of angiotensin I. A second run was made under identical conditions with the exception of increasing the capillary exit voltage of the interface from 80 to 155 V, to produce fragment ions from the eluting peptides and alteration of the m/z range to 200–1800. Data were converted to MassLynx (Micromass/Waters, Manchester, U.K.) format for analysis. All spectra were averaged into a single spectrum. This was subjected to analysis by MassLynx MaxENT3 to produce a list of mono-isotopic molecular weights for each deconvoluted component. This list was searched versus the protein sequence to determine possible peptides without any constraints on the cleavage sites. Use of a 5 ppm error window produced unambiguous results for most peptides. For ambiguous results, the spectrum was extracted from the high-capillary exit voltage run. The fragment ions present in the spectrum

were used to resolve the ambiguity by comparison to theoretical fragmentation patterns generated by the MassLynx software. Sequence coverage was 92% for p38 α and 96% for 6His–MK2a 51–400.

Deuterium Exchange in Deuterium Exchange Experiments. Protein was diluted 1:10 into deuterated 5 mM NaH₂PO₄ buffer (pH 7.0) and allowed to exchange for varying lengths of time (5, 15, 45, 100, and 1000 s) at room temperature. During the exchange, the concentration of protein was 10 μ M and the concentration of CMPD1 or CMPD2 was 50 μ M. The exchange reaction was quenched by lowering the pH and temperature of the reaction [an equal volume of ice-cold 100 mM NaH₂PO₄ (pH 2.5) was added]. Appropriate controls were also analyzed. The 0% control was protein that had not been exposed to D₂O. The 100% control was protein that had all exchangeable hydrogens replaced with deuterium. This was achieved by incubating the protein in 100% D₂O at an elevated temperature (60 °C overnight). The protein was then digested with pepsin (1:1 for 5 min on ice) and injected onto a 0.8 mm \times 150 mm C18 (Pepmap C18, LC Packings) column for separation by μ HPLC. The flow rate was 30 μ L/min with the injector, sample loop, column, and transfer lines placed in an ice bath.

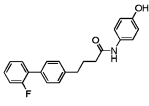
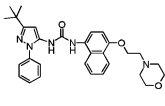
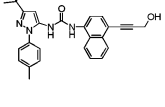
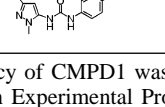
Mass Spectrometry in Deuterium Exchange Experiments. A Bruker ApexII FTMS apparatus with ESI was employed for on-line monitoring of the chromatographic effluent. A 1.1 s hexapole accumulation was performed before ion injection, excitation, and detection (m/z 350–2000). Two 256K spectra were averaged for each stored spectrum; 128 averaged spectra were acquired per run. The resolution was 40 000 fwhm. An external calibration with in-source fragment ions of angiotensin I was performed. The trapping and excitation values were optimized to reduce variation of mass assignment with ion population. The hexapole accumulation had the effect of integrating the ESI ions, and thus improving the measurement of relative abundance data. The capillary exit voltage was 70 V.

Data Analysis in Deuterium Exchange Experiments. Spectra from each time point were analyzed. For each identified peptide of interest, the spectrum within the LC–MS run corresponding to its elution was determined. A centroid of the most intense charge state of the peptide's molecular ion cluster was calculated by multiplying the mass by the intensity for each isotope of the cluster and dividing the sum of these values by the total intensity. The resulting data were plotted graphically for each peptide, yielding a map of protection for the protein. The 100 s time points were chosen to pictorially represent exchange of “native” MK2a and p38 α (each protein alone in solution). For p38 α /CMPD1, the 100 s exchange was repeated three times with two alternating control analyses. Viewer Lite 4.2 (Accelrys Inc.) was employed to map results onto the crystal structures.

RESULTS AND DISCUSSION

Potent active site inhibitors of p38, designed to block the phosphorylation of p38 effector molecules, are effective in inhibiting inflammatory cytokine production in cells. The prototypical ATP competitive inhibitor of p38 α and p38 β , SB203580, is reported to prevent the phosphorylation of effector molecules in an ATP competitive manner (7, 36). A second class of more potent and selective inhibitors of

Table 1: Inhibition of p38 α ^a

Compound	Structure	K_i^{app} (MK2a)	K_i^{app} (ATF-2)	K_d
CMPD1		330 nM	>20 μ M	\sim 1 μ M ^b
CMPD2		--	--	90 pM ^c
CMPD3		--	--	870 pM ^d
CMPD4		--	--	1.16 μ M ^c

^a The potency of CMPD1 was determined by steady-state kinetics as described in Experimental Procedures. ^b The K_d was estimated by isothermal calorimetry in Figure 1. ^c The potencies of the slow-tight binding inhibitor, CMPD2 (35), and CMPD4 (8) were measured by competition with the fluorescent inhibitor of p38 α , SKF 86002. ^d The potency of CMPD3 was measured by thermal denaturation as described in Experimental Procedures.

p38 α , represented by BIRB 796 and CMPD2 (Table 1), block the phosphorylation of multiple p38 α substrates. CMPD2 and BIRB 796 have been observed to inhibit p38 α by a slow-tight binding mechanism. BIRB 796 has also been observed to compete with ATP for p38 α by structural studies and by competition with a fluorescent ATP analogue (8). While the ATP competitive inhibitor classes prevent the production of TNF α in cell culture, they also block cellular functions not involved in cytokine production.

We have recently characterized a tight, functional, activated p38 α ·MK2a signaling complex, which is required for TNF α production, by steady-state kinetic and thermodynamic analyses (20). Inhibitors that prevent the phosphorylation and activation of MK2a were identified in a high-throughput screen and characterized to assess the feasibility of developing specific inhibitors of the p38 α ·MK2a signaling complex. A novel inhibitor, CMPD1 (Table 1), that blocks p38 α -dependent phosphorylation of MK2a, but does not block the phosphorylation of ATF-2 and MBP (data not shown), was discovered.

To determine the mechanism of inhibition of the substrate selective inhibitor, it was essential to identify the binding target of CMPD1 by isothermal titration calorimetry. CMPD1 was observed to bind to unphosphorylated p38 α , as shown in Figure 1. Because of insufficient solubility of CMPD1, an exact fit of K_d was not possible; however, the K_d is approximately 1 μ M. No evidence for an interaction between CMPD1 (20 μ M) and GST–MK2a was observed (data not shown). Thus, the data demonstrate that CMPD1 binds directly to p38 α to prevent the phosphorylation of MK2a.

The observations of p38 α binding and substrate selective inhibition by CMPD1 imply that this inhibitor is noncompetitive with ATP. To test this hypothesis, the phosphorylation of MK2a by activated p38 α at various ATP and CMPD1 concentrations was assessed. The reciprocal initial velocities were plotted versus the reciprocal ATP concentration to

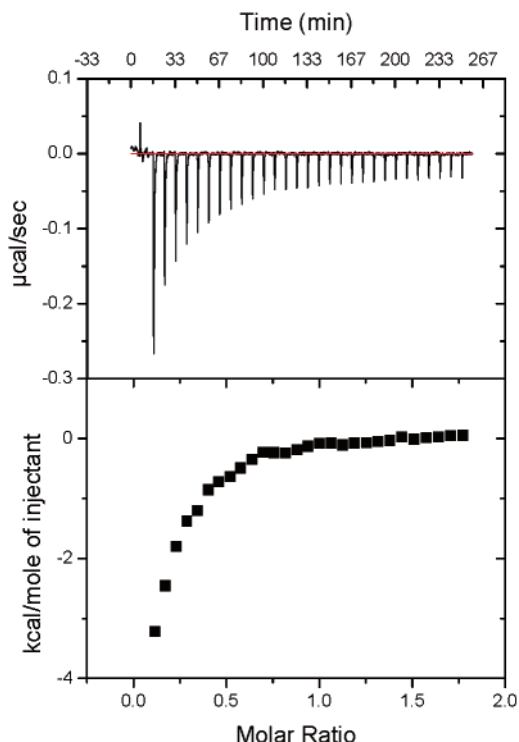


FIGURE 1: Isothermal titration calorimetry of binding of CMPD1 to p38 α . The procedure is described in Experimental Procedures.

generate a Lineweaver–Burk plot (Figure 2A), which was indicative of noncompetitive inhibition with ATP; CMPD1 reduced the observed V_{\max} at high concentrations of ATP. This is in contrast to an ATP competitive pattern of inhibition for known p38 inhibitors described previously (7, 36, 37). The initial rates of catalysis were then plotted versus the ATP concentration, and the data were fit globally to noncompetitive models of inhibition, in which inhibitor and substrate bind to separate sites on the enzyme. The best fits were obtained with the noncompetitive partial and mixed partial mechanism of inhibition, where the inhibitor (I) and substrate (S) do not compete with each other for the enzyme (E). The data were fit well by the noncompetitive partial inhibition model ($r^2 = 0.994$), where the ESI complex catalyzes product formation at a reduced rate compared to that of ES ($0.05V_{\max}$). The fit provided apparent values for K_M , V_{\max} , and K_i (Figure 2B). These values are apparent because multiple MK2a residues were phosphorylated (T222, S272, and T334) at similar rates by p38 α (20). The K_i^{app} for CMPD1 inhibition of the p38 α ·MK2a signaling complex was determined to be 330 nM; this affinity is similar to that observed with unactivated p38 α as measured by ITC. The data were also fit well by the mixed partial inhibition model ($K_i^{\text{app}} = 220$ nM; $r^2 = 0.996$), where the ESI complex catalyzes product formation at a reduced rate compared to that of ES ($0.06V_{\max}$), and the EI complex binds S with slightly reduced affinity compared to that of E ($1.9K_M$). Thus, CMPD1 binding may mildly perturb the binding of ATP to p38 α . Good fits to these noncompetitive mechanisms of inhibition are consistent with a mechanism in which CMPD1 binding perturbs the optimal transition-state orientation of substrates (MgATP and MK2a) and catalytic residues in the active site of p38 α .

The MK2a substrate selective and ATP noncompetitive characteristics of the CMPD1 inhibitor suggest that the

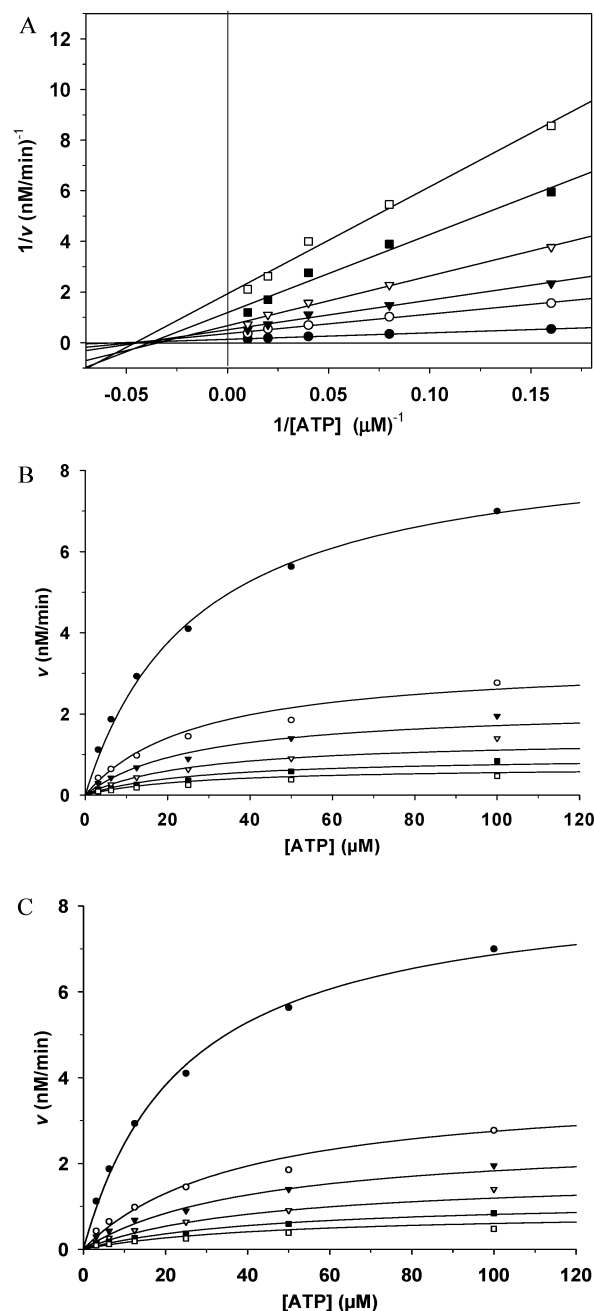


FIGURE 2: ATP noncompetitive inhibition of p38 α . The inhibition of p38 α by CMPD1, at constant MK2a ($1.8 \mu\text{M}$) and various ATP concentrations, was assessed. The average initial rate ($n = 3$) of p38 α (1 nM) catalysis was plotted vs the ATP concentration at each concentration of inhibitor. (A) A Lineweaver–Burk plot of the data was obtained by plotting the inverse initial velocity vs the inverse ATP concentration at the various concentrations of CMPD1: 0 (\bullet), 0.625 (\circ), 1.25 (\blacktriangledown), 2.5 (∇), 5 (\blacksquare), and $10 \mu\text{M}$ (\square). (B) The data were processed by a global curve fit to a noncompetitive partial mechanism of inhibition. The concentrations of CMPD1 were 0 (\bullet), 0.625 (\circ), 1.25 (\blacktriangledown), 2.5 (∇), 5 (\blacksquare), and $10 \mu\text{M}$ (\square). A fit to the noncompetitive partial mechanism ($r^2 = 0.994$) of inhibition yielded apparent values for V_{\max} ($8.8 \pm 0.2 \text{ nM/min}$), K_M ($27 \pm 2 \mu\text{M}$), K_i ($330 \pm 20 \text{ nM}$), and β (0.05 ± 0.01). (C) A fit to the mixed partial mechanism ($r^2 = 0.996$) of inhibition yielded apparent values for V_{\max} ($8.6 \pm 0.2 \text{ nM/min}$), K_M ($25 \pm 2 \mu\text{M}$), K_i ($220 \pm 30 \text{ nM}$), α (1.9 ± 0.4), and β (0.06 ± 0.01).

molecule may bind to the p38 α docking groove to perturb an interaction with the carboxy-terminal docking domain of MK2a. SPR experiments were conducted to determine whether CMPD1 abrogated or weakened the binding of p38 α

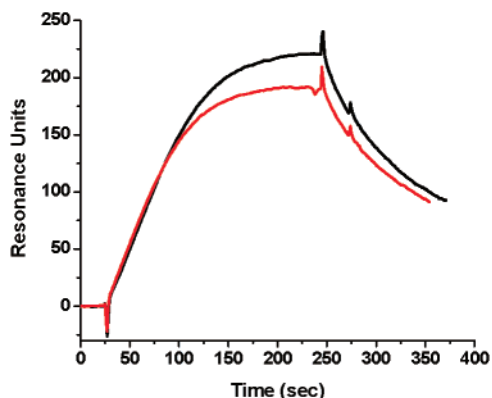


FIGURE 3: SPR measurement of binding of p38 α to MK2a in the presence of CMPD1. p38 α (5 nM) was injected over an MK2a surface for 220 s at 30 μ L/min in the absence (red) or presence of 1 μ M CMPD1 (black).

to immobilized GST–MK2a. The rate of p38 α ·MK2a complex formation was unaltered by 1 μ M CMPD1, as shown in Figure 3, and higher concentrations of CMPD1 (up to 10 μ M) did not prevent the binding of p38 α to MK2a observed by SPR (data not shown). Thus, no evidence which suggests that CMPD1 precludes the interaction between the docking groove of p38 α and the docking domain of MK2a was obtained. It is still possible that CMPD1 binding alters the position of MK2a at the active site to reduce the rate of catalysis of MK2a phosphorylation without significantly reducing the binding affinity of MK2a for p38 α .

CMPD3, a fluorescent analogue of the slow-tight binding p38 α inhibitor, BIRB 796 (8), was used in a competitive binding assay with CMPD1 to further test the nature of CMPD1 inhibition (Figure 4). As described previously (8), the fluorescent analogue of BIRB 796 binds slowly with picomolar affinity to p38 α in an ATP competitive fashion. ATP competitive inhibitors of p38 α will slow the rate of binding of this fluorescent analogue. Allosteric inhibitors that compete with CMPD3, such as CMPD4, which has been shown to bind with a lower affinity ($K_d = 1.16 \mu$ M) in the allosteric pocket of p38 α (8), also slow the rate of binding of CMPD3 to p38 α (Figure 4). CMPD1 caused a slight alteration to the rate of complex formation between the fluorescent analogue of BIRB 796 and p38 α . This observation is consistent with partial overlap of the binding sites of these compounds or allosteric effects. A similar alteration was observed when activated p38 α was employed. This is consistent with the observation above that activation of p38 α does not greatly affect the binding of CMPD1.

To identify the binding site of the substrate selective inhibitor and gain additional information pertaining to the mechanism of inhibition, DXMS studies of the signaling complex (p38 α ·MK2a) and inhibitory complexes (p38 α ·CMPD1 and p38 α ·CMPD2) were undertaken. The DXMS behavior of both p38 α and MK2a was determined at several time points. Results for the 100 s time point were mapped onto the structure of p38 α (17), as shown in Figure 5. This provides a graphical representation of the rough correlation between solvent accessibility and D₂O exchange rates, as expected. The results for a similar experiment with MK2a are shown in Figure 6. Again, a rough correlation exists between exchange rates and solvent accessibility. These results serve as control data for the experiments involving

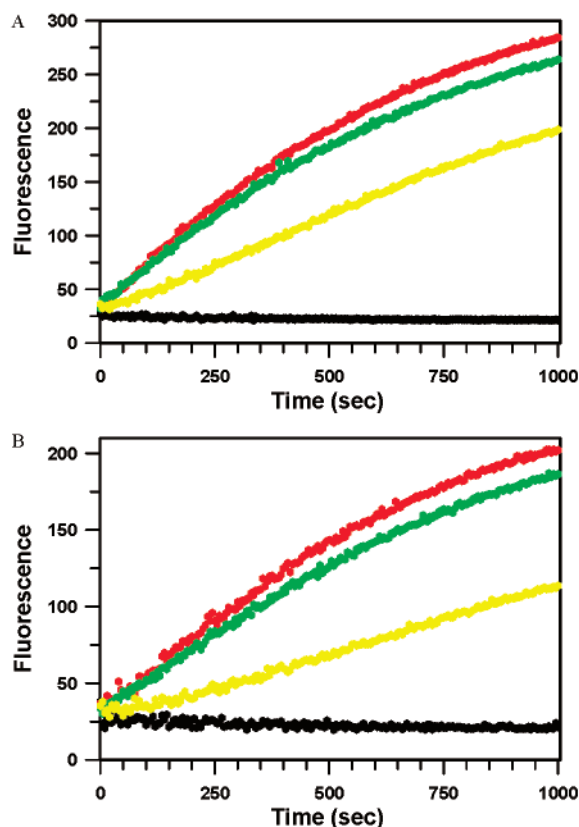


FIGURE 4: Fluorescence p38 α binding assay. (A) The binding of CMPD3 (500 nM), a close structural analogue of CMPD2, to p38 α (170 nM) resulted in an increase in the fluorescence of this probe (red) as described in Experimental Procedures. In the absence of p38 α , CMPD3 (500 nM) did not exhibit an increase in fluorescence (black). The binding of CMPD3 (500 nM) to p38 α (170 nM) in the presence of CMPD1 (5 μ M) was slightly perturbed (green), and the binding of CMPD3 (500 nM) to p38 α (170 nM) was significantly slowed in the presence of CMPD4 (5 μ M) that binds in the allosteric pocket occupied by CMPD3 and BIRB 796 (8). (B) The binding of compounds to activated p38 α was monitored as described for panel A.

alterations of exchange rates upon formation of the p38 α ·MK2a complex and the binding of inhibitors to p38 α .

Figure 7 displays the alteration of exchange rates for MK2a produced by complex formation with p38 α mapped onto the published crystal structure of MK2a (38). The most extensive changes are seen in the carboxy-terminal regulatory domain. The structure of a catalytically active truncation of MK2a has also been reported (39). Protection from exchange in this region is consistent with tight binding to the recognition site of p38 α , as shown by the peptide binding experiments (18). The electron density in the reported crystal structure of MK2a ends at residue 377, while we observe significant protection in MK2a residues 384–395, consistent with contact between this region and p38 α . The strongest protection was observed in a region (MK2a residues 363–383) that lies between the nuclear localization signal (MK2a residues 385–389) and the nuclear export signal that mediates translocation of p38 α and MK2 α to the cytoplasm upon stimulation (10, 14). The nuclear export signal of MK2a, comprising residues 353–368, is represented by residues 355–360, which coincide with high levels of protection. Phosphorylation of MK2a at residue T334 by p38 α is reported to disrupt the interaction between kinase and carboxy-terminal regulatory domains, making the nuclear

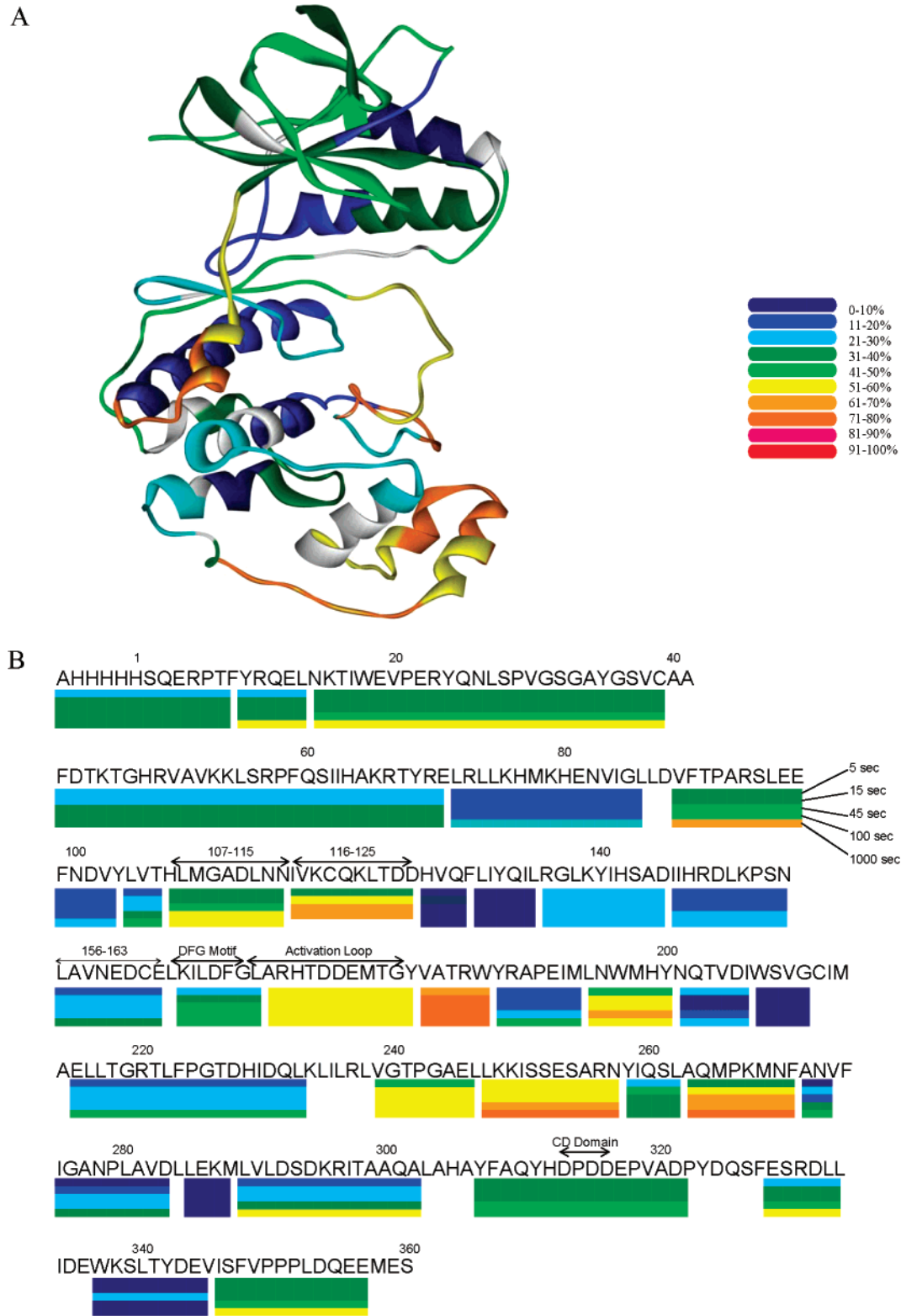


FIGURE 5: DXMS analysis of p38 α . (A) Extent of D₂O exchange at the 100 s time point mapped onto the published crystal structure of p38 α . (B) The data for all time points were mapped onto the sequence of p38 α . The percent exchange was calculated as the change in average mass between each exchanged peptide and the same peptide with no exchange divided by the number of exchangeable amide H. This figure also denotes the peptides studied for each protein.

export signal available for nuclear receptor binding. Weaker levels of protection are also observed in the α J and α K helix regions, which include the MK2a phosphorylation site (T334), demonstrating direct or allosteric effects in these regions produced by p38 α binding. No significant protection was observed in the region spanning the activation loop of

MK2a (residues 211–246) or in the region of S272. Residues T222 and S272 are both phosphorylated efficiently by p38 α (20).

Figure 8 shows the alteration of D₂O exchange rates of p38 α produced by MK2a binding. The most significant levels of protection are observed in an area containing p38 α

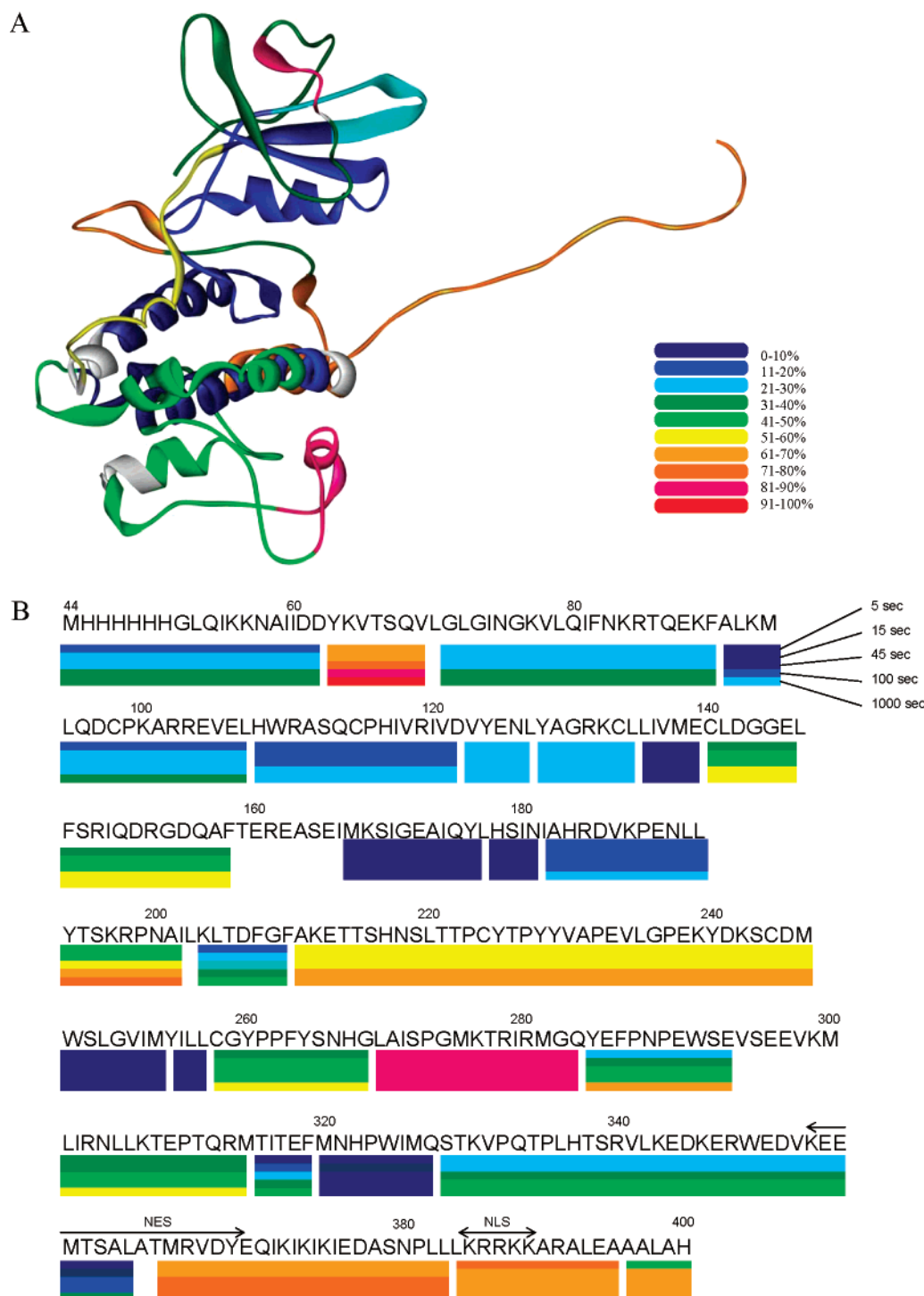


FIGURE 6: DXMS analysis of MK2a. (A) Extent of D_2O exchange at the 100 s time point mapped onto the published crystal structure of MK2a. (B) The data for all time points were mapped onto the sequence of MK2a. The percent exchange was calculated as described in the legend of Figure 5.

residues 107–115, 116–125, and 156–163. Residues 107–115 form a significant portion of the nucleotide binding pocket. We also observe protection at residues 9–13. These observations are in general agreement with recently published (40) DXMS results obtained by binding a peptide (SKGK-SKRKKDLRISCNSK) derived from MKK3b with p38. That study found protection in analogous regions, and additional protection near the N-terminus and near the C terminus. They also observed effects, not relevant to this discussion, due to formation of a disulfide bond to Cys162 of p38. MK2a does not have a cysteine residue analogous to that of the MKK3b-

derived peptide. The backbone amide N of residue M109 forms a hydrogen bond with the purine ring of ATP at one side of the pocket (41). The reductions in the exchange rates of the nucleotide binding pocket residues are probably not due to direct interactions with MK2a residues, as this could occlude binding of MgATP to this site; instead, the DXMS effects are more likely caused by an MK2a-induced conformational change of these residues. p38 α residues 116–125 and 156–163 coincide with the protein substrate binding groove described by X-ray crystallography of p38 α cocrystallized with peptides derived from MEF2A and MKK3b

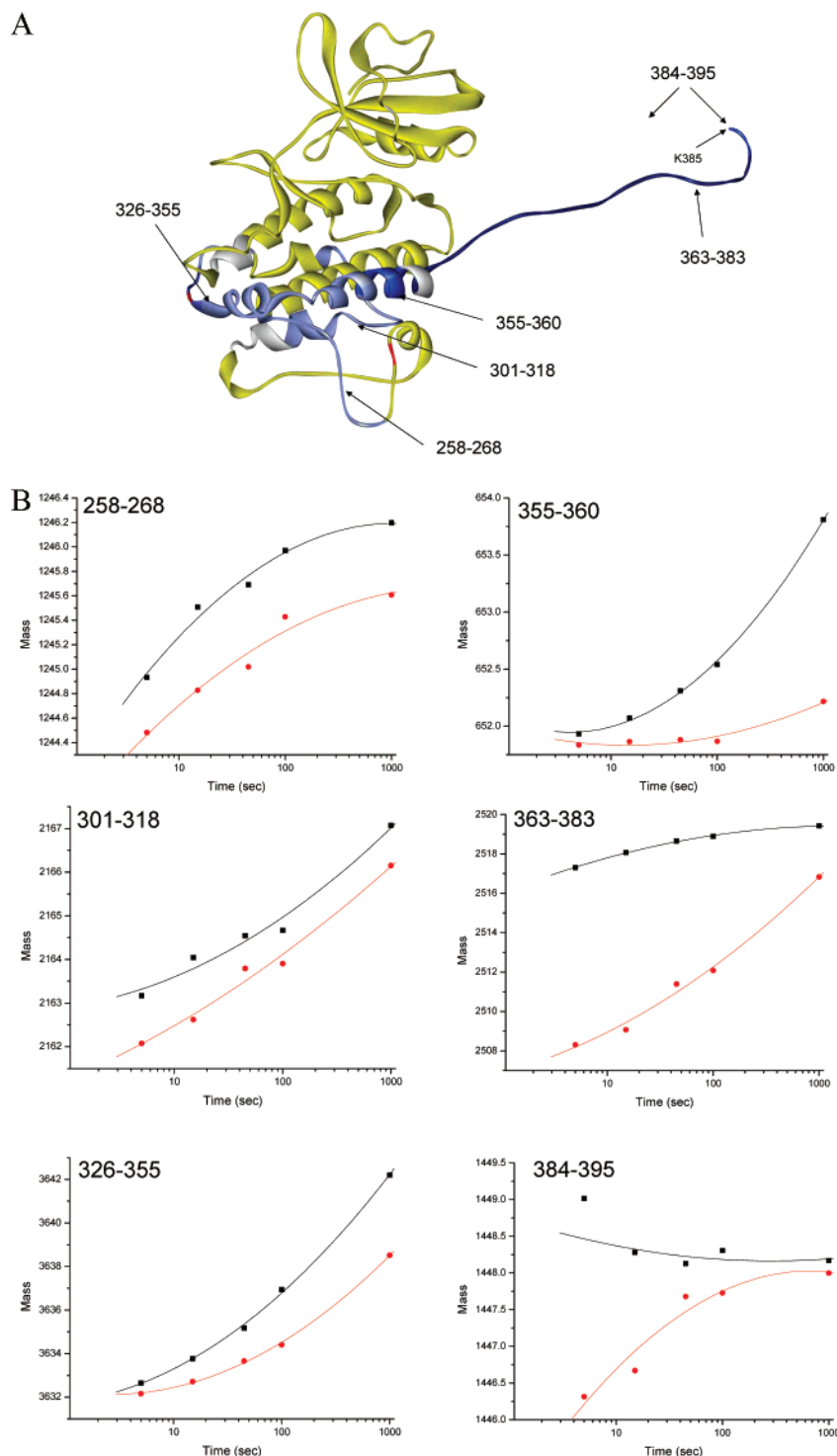


FIGURE 7: DXMS analysis of MK2a complexed with p38 α . (A) Protection from D₂O exchange for MK2a when complexed with p38 α mapped onto the structure of MK2a. Light blue regions indicate moderate protection, while dark blue regions indicate stronger protection when compared with the control analysis of MK2a without p38. Red amino acids denote phosphorylation sites S272 and T334. A third residue of the activation loop, T222, phosphorylated by p38 α is not labeled, because the activation loop is disordered. (B) Data at each time point, showing the average mass measured for control MK2a (black) and MK2a complexed with p38 (red) for several peptides that showed significant alteration of exchange, are displayed graphically.

(18). The reductions in exchange rates for this docking groove region are likely due to a tight interaction with the carboxy-terminal docking residues (370–400) of MK2a (20). This tight interaction between the docking domain of MK2a and the docking groove of p38 α has been observed to be essential for efficient phosphorylation of residues required for activation of MK2a (T222 and S272) and nuclear export (T334) of the signaling partners (20, 25). The orientation of

binding of the carboxy-terminal MK2a docking domain in the p38 α docking groove has not been determined. Noteworthy is the lack of protection observed for the region that includes acidic p38 α residues 313–316 that are part of the CD domain. This is consistent with work (18) that determined the structure of p38–peptide cocrystals with peptides derived from MEF2A and MKK3b. The exact structure of the p38 α ·MK2a complex has not been determined.

A

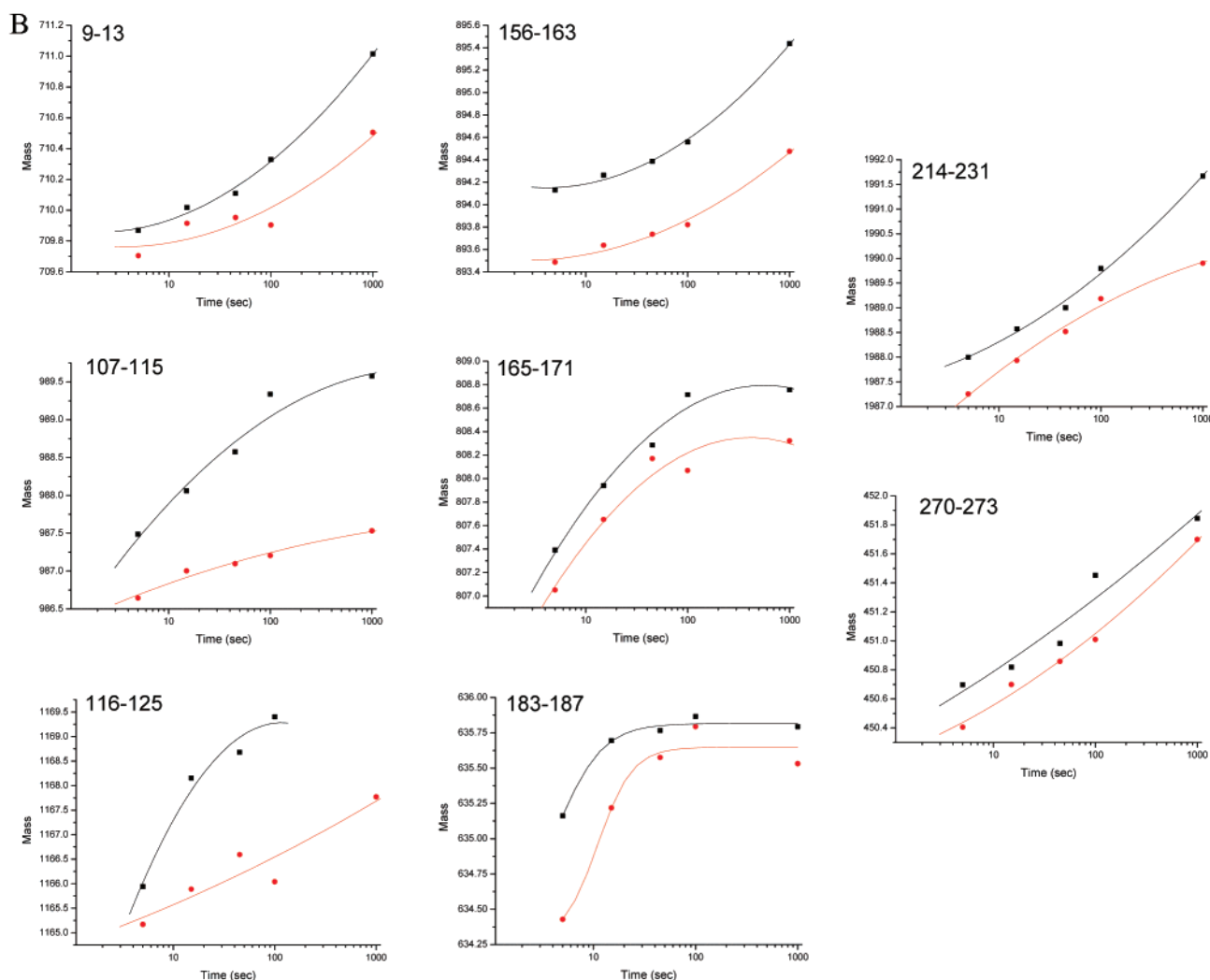
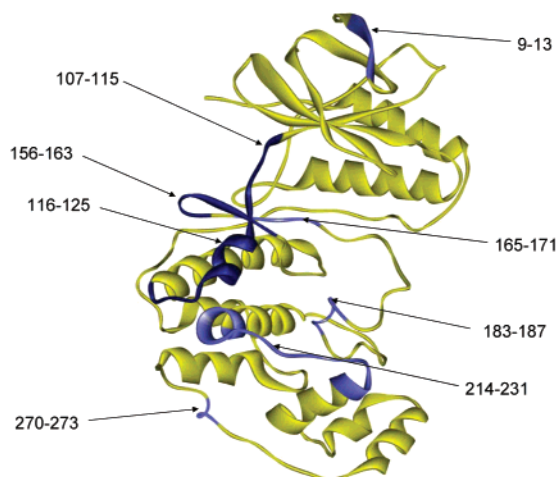
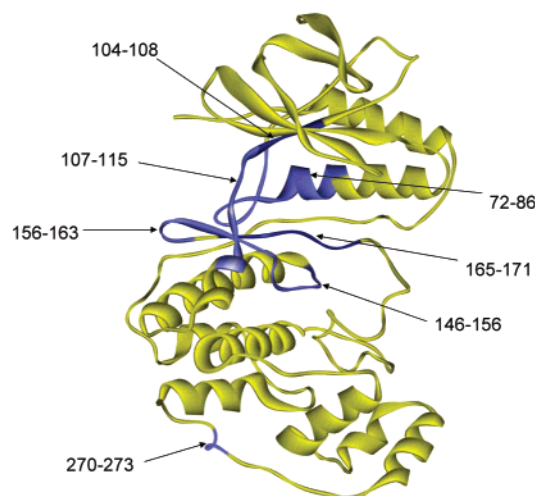


FIGURE 8: DXMS analysis of p38 α complexed with MK2a. (A) Protection of p38 α from D₂O exchange when complexed with MK2a mapped onto the structure of p38 α . Light blue regions indicate moderate protection, while dark blue regions indicate strong protection. (B) Average mass for peptides showing significant protection between control p38 α (black) and p38 α complexed with MK2a (red).

Other regions of p38 α that exhibit weaker levels of protection due to MK2a binding are also shown in Figure 8. These include the DFG motif contained in p38 α residues 165–171. The DFG motif located within the p38 α peptide (165–171) perturbed by MK2a binding is important for catalytic and inhibitory mechanisms. This DFG motif has been shown (8) to change conformation upon binding of BIRB 796 in a manner which allosterically alters the ATP

binding site. Residue D168 of this loop also corresponds to D171 of p38 γ , which has been observed by X-ray crystallography to be a first-coordination sphere ligand of nucleotide-bound Mg²⁺ ion found in the active site of p38 γ (42). The positions of this nucleotide-bound divalent cation and the conserved aspartate residue are predicted to be essential for optimal catalytic efficiency. The orientation of the nucleotide-bound divalent cation by aspartate of the DFG

A



B

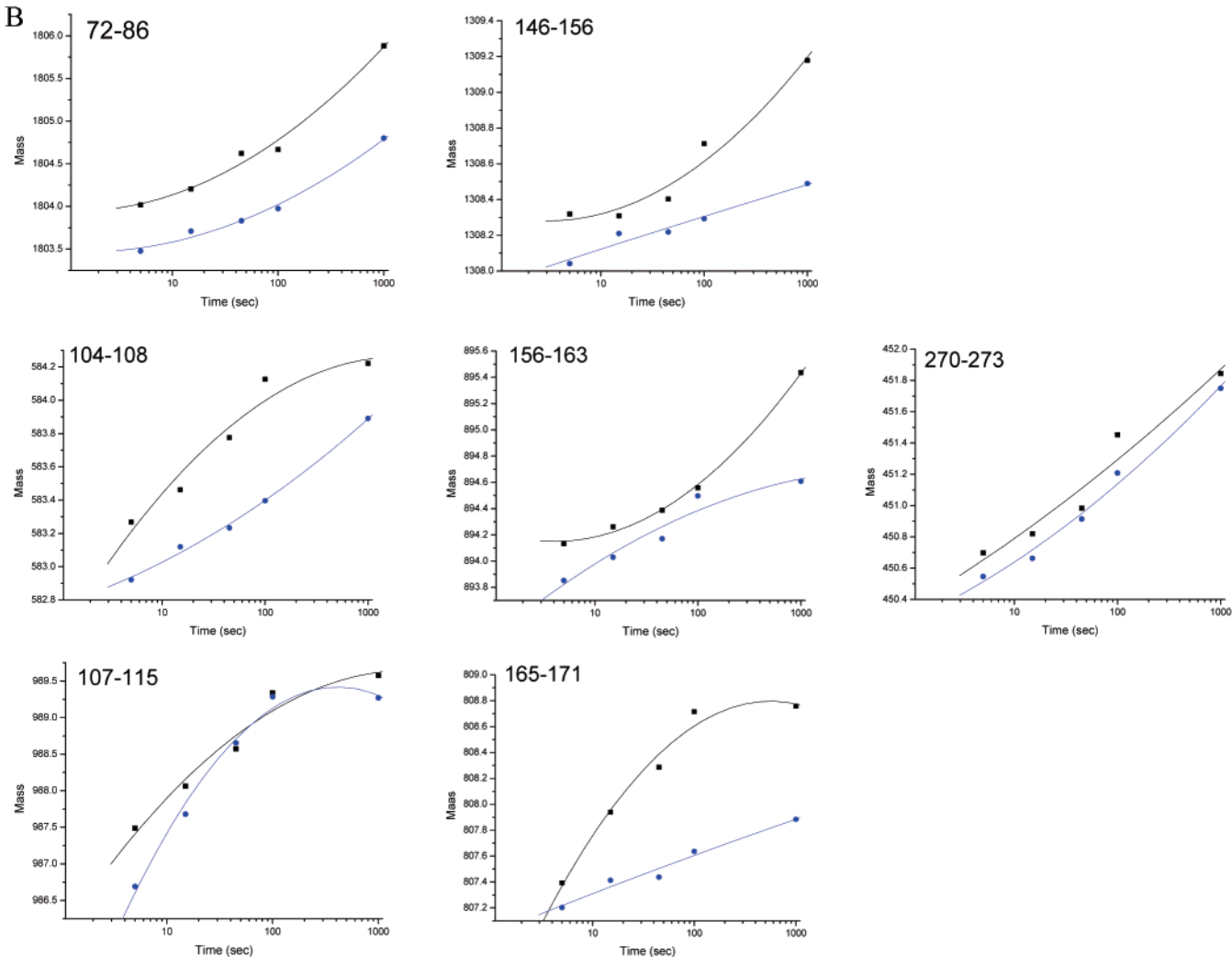
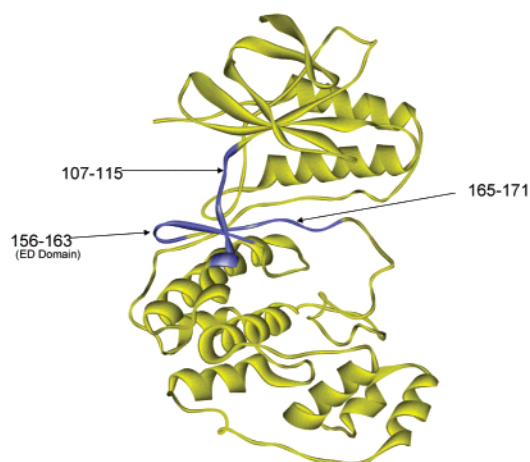


FIGURE 9: DXMS analysis of p38 α complexed with CMPD2. (A) Protection of p38 α from D₂O exchange when complexed with CMPD2 mapped onto the structure of p38 α . Light blue regions indicate moderate protection, while dark blue regions indicate strong protection. The crystallography contacts of BIRB 796 are indicated. (B) Average mass for peptides showing significant protection between control p38 α (black) and p38 α complexed with CMPD2 (blue).

loop is not unique to the p38 family of enzymes. The crystal structures of well-characterized kinases, such as cAMP-dependent protein kinase (43) and pyruvate kinase (44), indicate that the conserved aspartate residues of these enzymes reside in the first coordination sphere of the divalent

cation that is liganded by the β - and γ -phosphoryl groups of the nucleotide substrate. The results suggest that binding of MK2a to p38 α results in conformational changes to the DFG loop that could be required for optimizing the catalytic efficiency of MK2a phosphorylation.

A



B

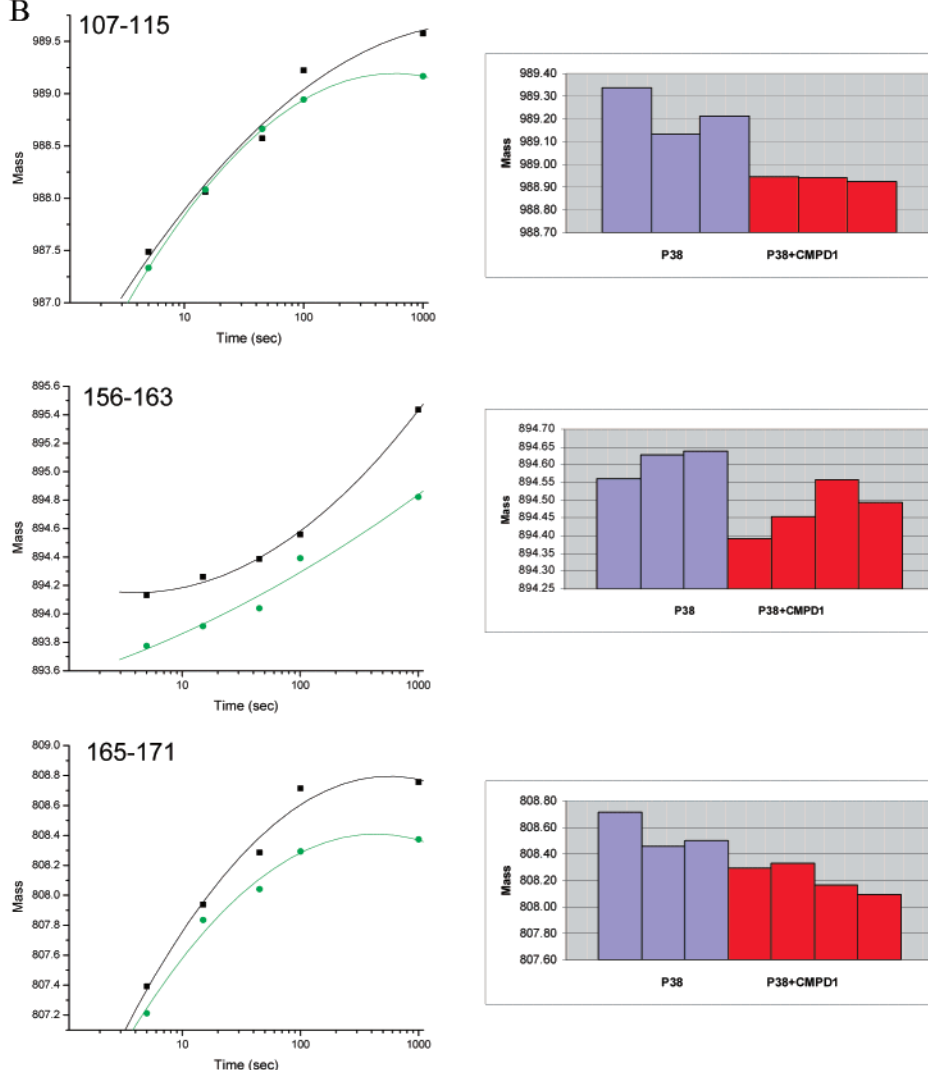


FIGURE 10: DXMS analysis of p38 α complexed with CMPD1. (A) Protection of p38 α from D₂O exchange when complexed with CMPD1 mapped onto the published crystal structure of p38 α . Light blue regions indicate weak protection, while dark blue regions indicate moderate protection. (B) Measured average mass at each time point for peptides showing significant alteration between control p38 α (black) and CMPD1 complexed with p38 α (green). For the relatively weak effects of CMPD1, the average mass results for repetitive 100 s exchange of control p38 α (blue bars) and p38 α complexed with CMPD1 (red bars) are shown next to the corresponding peptides. The color scheme for weak, strong, or moderate protection was arbitrarily selected to aid in viewing the results.

Thus, the DXMS protection seen in p38 α and MK2a upon complex formation maps onto published structures in a manner consistent with tight binding between the p38 α docking groove and the carboxy terminus of MK2a. Ad-

ditional protection in both molecules is consistent with additional binding contacts and/or extensive allosteric effects. The affected regions include the nuclear localization and export signals of MK2a, the nucleotide binding pocket of

p38 α , and the DFG loop of p38 α . The numerous effects observed upon complex formation suggest that opportunities exist for substrate selective inhibition of p38 α .

Figure 9 shows the protection of p38 α provided by binding of the ATP competitive inhibitor, CMPD2. The X-ray crystallographic structure of a cocrystal of p38 α and the close analogue of CMPD2 (BIRB0796) has been published (8). CMPD2-dependent protection in p38 α regions containing residues 72–86, 104–108, 156–163, and 165–171 directly coincides with contact observed by X-ray crystallography of BIRB 796.

It was particularly interesting to compare the results obtained with CMPD2 with the D₂O exchange behavior of the substrate selective inhibitor (CMPD1). The DXMS method provided binding site data in this system that we did not find amenable to formation of a cocrystal for X-ray crystallographic analysis. As shown in Figure 10, CMPD1 produced lower levels of protection from exchange, as anticipated for a relatively weak binder. To verify these effects, multiple analyses were conducted at the 100 s time point (Figure 10B). Excellent precision in mass measurement was obtained, due to the use of FTMS. The results of this experiment mapped onto the structure of p38 α are shown in Figure 10. The observed protection of p38 α residues 107–115, 156–163, and 165–171 is a subset of the effects observed upon the binding of the ATP competitive inhibitor, CMPD2. This is consistent with CMPD1 binding in the same vicinity as CMPD2, with some common binding interactions. While the exact binding site of CMPD1 is not completely defined by DXMS analysis, the data combined with those obtained from kinetic and fluorescence competition studies suggest that the ATP noncompetitive, MK2a selective inhibitor binds near the active site, but outside of the nucleotide pocket and with only partial overlap of the pocket occupied by BIRB 796 and CMPD2 (8). This observation raises the concern that commercial efforts to alter the structure of CMPD1 to enhance binding may produce interactions that negate the substrate selective properties of the molecule.

The results suggest that CMPD1 binding in the active site region of p38 α induces perturbations that may result in the suboptimal positioning of substrates and metal ion cofactors in the transition state, resulting in selective inhibition of the p38 α ·MK2a complex. The protection of p38 α residues 156–163 by CMPD1 was weaker than that observed with CMPD2, but was still significant. This region includes the ED domain acidic residues that have been shown by mutagenesis (15) to specifically regulate the docking of MK3, a closely related substrate to MK2a. CMPD2 may also perturb MK2a binding selectively through the ED domain of p38 α , but this would be obscured by exclusion of ATP from the active site and subsequent catalytic inhibition.

Alterations to the positions of ATP and the DFG loop in the transition state induced by CMPD1 might also contribute to the observed decrease in catalytic efficiency. The slight perturbation of the nucleotide binding pocket residues observed by DXMS may lead to a misalignment of ATP in the transition state of MK2a phosphorylation. If this perturbation contributes to the distinct mechanism of CMPD1 inhibition, it must be subtle, because large perturbations in this pocket would be expected to prevent p38 α -dependent catalysis of the phosphorylation of many more substrates,

including ATF-2. Subtle alterations in the DFG loop region, which contains the divalent cation binding residue (D168), could also contribute to the specific inhibition of MK2a phosphorylation by p38 α ; CMPD1 could perturb the position of MgATP relative to MK2a in the transition state. Again, major displacement of the DFG loop would likely prevent the phosphorylation of all substrates.

The DXMS method has detected subtle perturbations in regions of p38 α , containing the ED domain and other active site residues, that begin to explain how CMPD1 specifically inhibits the function of the p38 α ·MK2a signaling complex.

Conclusion. A substrate selective p38 α inhibitor of MK2a phosphorylation has been discovered. This inhibitor has been shown to bind to p38 α and not MK2a by ITC, and the inhibitor was observed to be noncompetitive with ATP. SPR experiments indicate that it does not operate by prevention of formation of the p38 α ·MK2a complex. DXMS measurements are consistent with binding of the inhibitor in the vicinity of the active site where non-substrate selective inhibitors bind, and with a mechanism of inhibition in which alterations to catalytic residues and substrates in the transition state lead to reduced rates of MK2a phosphorylation.

ACKNOWLEDGMENT

We are indebted to Kate Makai for her help in processing the mass spectrometric data.

REFERENCES

1. Dinarello, C. A. (1991) Inflammatory cytokines: interleukin-1 and tumor necrosis factor as effector molecules in autoimmune diseases, *Curr. Opin. Immunol.* 3, 941–948.
2. Feldmann, M., Brennan, F. M., and Maini, R. N. (1996) Role of cytokines in rheumatoid arthritis, *Annu. Rev. Immunol.* 14, 397–440.
3. Rankin, E. C., Choy, E. H., Kassimos, D., Kingsley, G. H., Sopwith, A. M., Isenberg, D. A., and Panayi, G. S. (1995) The therapeutic effects of an engineered human anti-tumor necrosis factor alpha antibody (CDP571) in rheumatoid arthritis, *Br. J. Rheumatol.* 34, 334–342.
4. Nuki, K. G., Bresnihan, B., Bear, M. B., and McCabe, D. (2002) Long-term safety and maintenance of clinical improvement following treatment with anakinra (recombinant human interleukin-1 receptor antagonist) in patients with rheumatoid arthritis: extension phase of a randomized, double-blind, placebo-controlled trial, *Arthritis Rheum.* 46, 2838–2846.
5. Weinblatt, M. E., Kremer, J. M., Bankhurst, A. D., Bulpitt, K. J., Fleischmann, R. M., Fox, R. I., Jackson, C. G., Lange, M., and Burge, D. J. (1999) A trial of etanercept, a recombinant tumor necrosis factor receptor: Fc fusion protein, in patients with rheumatoid arthritis receiving methotrexate, *N. Engl. J. Med.* 340, 253–259.
6. Jarvis, B., and Faulds, D. (1999) Etanercept: a review of its use in rheumatoid arthritis, *Drugs* 57, 945–966.
7. Lee, J. C., Badger, A. M., Griswold, D. E., Dunnington, D., Truneh, A., Votta, B., White, J. R., Young, P. R., and Bender, P. E. (1993) Bicyclic imidazoles as a novel class of cytokine biosynthesis inhibitors, *Ann. N.Y. Acad. Sci.* 696, 149–170.
8. Pargellis, C., Tong, L., Churchill, L., Cirillo, P. F., Gilmore, T., Graham, A. G., Grob, P. M., Hickey, E. R., Moss, N., Pav, S., and Regan, J. (2002) Inhibition of p38 MAP kinase by utilizing a novel allosteric binding site, *Nat. Struct. Biol.* 9, 268–272.
9. Hannigan, M. O., Zhan, L., Ai, Y., Kotlyarov, A., Gaestel, M., and Huang, C. K. (2001) Abnormal migration phenotype of mitogen-activated protein kinase-activated protein kinase 2^{-/-} neutrophils in zigmund chambers containing formyl-methionyl-leuc-phenylalanine gradients, *J. Immunol.* 167, 3953–3961.
10. Kotlyarov, A., Yannani, Y., Fritz, S., Laass, K., Telliez, J.-B., Pitman, D., Liu, L.-L., and Gaestel, M. (2002) Distinct cellular functions of MK2, *Mol. Cell. Biol.* 22, 4827–4835.

11. Kontoyiannis, D., Boulougouris, G., Manoloukos, M., Armaka, M., Apostolaki, M., Pizarro, T., Kotlyarov, A., Forster, I., Flavell, R., Gaestel, M., Tsichlis, P., Cominelli, F., and Kollias, G. (2002) Genetic dissection of the cellular pathways and signaling mechanisms in modeled tumor necrosis factor-induced Crohn's-like inflammatory bowel disease, *J. Exp. Med.* **196**, 1563–1574.
12. Wang, X., Xu, L., Wang, H., Young, P. R., Gaestel, M., and Feurstein, G. Z. (2002) Mitogen-activated protein kinase-activated protein (MAPKAP) kinase 2 deficiency protects brain from ischemic injury in mice, *J. Biol. Chem.* **277**, 43968–43972.
13. Shi, Y., and Gaestel, M. (2002) In the cellular garden of forking paths: how p38 MAPKs signal for downstream assistance, *Biol. Chem.* **383**, 1519–1536.
14. Tanoue, T., Moriguchi, A. M., and Nishida, E. (2000) A conserved docking motif in MAP kinases common to substrates, activators and regulators, *Nat. Cell Biol.* **2**, 110–116.
15. Tanoue, T., Maeda, R., Adachi, M., and Nishida, E. (2001) Identification of a docking groove on ERK and p38 MAP kinases that regulates the specificity of docking interactions, *EMBO J.* **20**, 466–479.
16. Wilson, K. P., Fitzgibbon, M. J., Caron, P. R., Griffith, J. P., Chen, W., McCaffrey, P. G., Chamber, S. P., and Su, M. (1996) Crystal structure of p38 mitogen-activated protein kinase, *J. Biol. Chem.* **271**, 27696–27700.
17. Wang, Z., Harkins, P. C., Ulevitch, R. J., Han, J., Cobb, M. H., and Goldsmith, E. J. (1997) The structure of mitogen-activated protein kinase p38 at 2.1 Å resolution, *Proc. Natl. Acad. Sci. U.S.A.* **94**, 2327–2332.
18. Chang, C., Xu, B., Akella, R., Cobb, M. H., and Goldsmith, E. J. (2002) Crystal structures of MAP kinase p38 complexed to the docking sites on its nuclear substrate MEF2A and activator MKK3b, *Mol. Cell* **9**, 1241–1249.
19. Kotlyarov, A., Neininger, A., Schubert, C., Eckert, R., Birchmeier, C., Volk, H. D., and Gaestel, M. (1999) MAPKAP kinase 2 is essential for LPS-induced TNF- α biosynthesis, *Nat. Cell Biol.* **1**, 94–97.
20. Lukas, S. M., Kroe, R. R., Wildeson, J., Peet, G. W., Frego, L., Davidson, W., Ingraham, R. H., Pargellis, C. A., Labadia, M. E., and Werneburg, B. G. (2004) Catalysis and function of the p38 α -MK2a signaling complex, *Biochemistry* **43**, 9950–9960.
21. Neiniger, A., Kontoyiannis, D., Kotlyarov, A., Winzen, R., Eckert, R., Volk, H. D., Holtmann, H., Kollias, G., and Gaestel, M. (2002) MK2 targets AU-rich elements and regulates biosynthesis of tumor necrosis factor and interleukin-6 independently at different post-transcriptional levels, *J. Biol. Chem.* **277**, 3065–3068.
22. Ben-Levy, R., Leighton, I. A., Doza, Y. N., Attwood, P., Morrice, N., Marshall, C. J., and Cohen, P. (1995) Identification of novel phosphorylation sites required for activation of MAPKAP kinase-2, *EMBO J.* **14**, 5920–5930.
23. Mahtani, K. R., Brook, M., Dean, J. L., Sully, G., Saklatvala, J., and Clark, A. R. (2001) Mitogen-activated protein kinase p38 controls the expression and posttranslational modification of tristetraprolin, a regulator of tumor necrosis factor alpha mRNA stability, *Mol. Cell. Biol.* **21**, 6461–6469.
24. Ben-Levy, R., Hooper, S., Wilson, R., Peterson, H. F., and Marshall, C. J. (1998) Nuclear export of the stress-activated protein kinase p38 mediated by its substrate MAPKAP kinase-2, *Curr. Biol.* **8**, 1049–1057.
25. Engel, K., Kotlyarov, A., and Gaestel, M. (1998) Leptomycin B-sensitive nuclear export of MAPKAP kinase 2 is regulated by phosphorylation, *EMBO J.* **17**, 3363–3371.
26. Neineinger, A., Theilemann, H., and Gaestel, M. (2001) FRET-based detection of different conformations of MK2, *EMBO Rep.* **21**, 703–708.
27. Zhang, Z. Q., and Smith, D. L. (1993) Determination of amide hydrogen exchange by mass spectrometry: A new tool for protein structure elucidation, *Protein Sci.* **2**, 522–531.
28. Zhang, Z. Q., Post, C. B., and Smith, D. L. (1996) Amide hydrogen exchange determined by mass spectrometry: application to rabbit muscle aldolase, *Biochemistry* **35**, 779–791.
29. Resing, K. A., and Ahn, N. G. (1998) Deuterium exchange mass spectrometry as a probe of protein kinase activation. Analysis of wild type and constitutively active mutants of MAP kinase kinase-1, *Biochemistry* **37**, 463–475.
30. Resing, K. A., Hoofnagle, A. N., and Ahn, N. G. (1999) Modeling deuterium exchange behavior of ERK2 using peptide mapping to probe secondary structure, *J. Am. Soc. Mass Spectrom.* **10**, 685–702.
31. Hoofnagle, A. N., Resing, K. A., Goldsmith, E. J., and Ahn, N. G. (2001) Changes in protein conformational mobility upon activation of extracellular regulated protein kinase-2 as detected by hydrogen exchange, *Proc. Natl. Acad. Sci. U.S.A.* **98**, 956–961.
32. Ehring, H. (1999) Hydrogen exchange-electrospray ionization mass spectrometry studies of structural features of proteins and protein/protein interactions, *Anal. Biochem.* **267**, 252–259.
33. Englander, J. J., Del Mar, C., Englander, S. W., Kim, J. S., Stranz, D. D., Hamuro, Y., and Woods, V. (2003) Protein structure change studied by hydrogen–deuterium exchange, functional labeling and mass spectrometry, *Proc. Natl. Acad. Sci. U.S.A.* **100**, 7057–7062.
34. Hamuro, Y., Wong, L., Shaffer, J., Kim, J. S., Stranz, D. D., Jennings, P. A., Woods, V. L., and Adam, J. A. J. (2002) Phosphorylation-driven motions in the COOH-terminal Src kinase, Csk, revealed by enhanced hydrogen–deuterium exchange and mass spectrometry, *J. Mol. Biol.* **3**, 871–881.
35. Kroe, R. R., Regan, J., Proto, A., Peet, G. W., Roy, T., Landro, L. D., Fuschetto, N. G., Pargellis, C. A., and Ingraham, R. H. (2003) Thermal denaturation: a method to rank slow binding, high-affinity p38 α MAP kinase inhibitors, *J. Med. Chem.* **46**, 4669–4675.
36. LoGrasso, P. V., Frantz, B., Rolando, A. M., O'Keefe, S. J., Hermes, J. D., and O'Neill, E. A. (1997) Kinetic mechanism for p38 MAP kinase, *Biochemistry* **36**, 10422–10427.
37. Frantz, B., Klatt, T., Pang, M., Parsons, J., Rolando, A., Williams, H., Tocci, M. J., O'Keefe, S. J., and O'Neil, E. A. (1998) The activation state of p38 mitogen-activated protein kinase determines the efficiency of ATP competition for pyridinylimidazole inhibitor binding, *Biochemistry* **37**, 13846–13853.
38. Meng, W., Swenson, L. L., Fitzgibbon, M. J., Hayakawa, K., Haar, E., Behrens, A. E., Fulghum, J. R., and Lippke, J. A. (2002) Structure of mitogen-activated protein kinase-activated protein (MAPKAP) kinase 2 suggests a bifunctional switch that couples kinase activation with nuclear export, *J. Biol. Chem.* **277**, 37401–37405.
39. Underwood, K. W., Parris, K. D., Federico, E., Mosyak, L., Czerwinski, R. M., Shane, T., Taylor, M., Svenson, K., Liu, Y., Hsiao, C.-L., Wolfson, S., Maguire, M., Malakian, K., Telliez, J.-B., Lin, L.-L., Kriz, R. W., Sehra, J., Somers, W. S., and Stahl, M. L. (2003) Catalytically active MAP KAP kinase 2 structures in complex with staurosporine and ADP reveal differences with the autoinhibited enzyme, *Structure* **11**, 627–636.
40. Lee, T., Hoofnagle, A. N., Kabuyama, Y., Stroud, J., Min, X., Goldsmith, E. J., Resing, K. A., and Ahn, N. G. (2004) Docking motif interactions in MAP kinases revealed by hydrogen exchange mass spectrometry, *Mol. Cell* **14**, 43–55.
41. Tong, L., Pav, S., White, D. M., Rogers, S., Crane, K. M., Cywin, C. L., Brown, M. L., and Pargellis, C. A. (1997) A highly specific inhibitor of human p38 MAP kinase binds in the ATP pocket, *Nat. Struct. Biol.* **4**, 311–316.
42. Bellon, S., Fitzgibbon, M. J., Fox, T., Hsiao, H.-M., and Wilson, K. P. (1999) The structure of phosphorylated p38 γ is monomeric and reveals a conserved activation-loop conformation, *Structure* **7**, 1057–1065.
43. Bossemeyer, D., Engh, R. A., Kinzel, V., Ponstingl, H., and Huber, R. (1993) Phosphotransferase and substrate binding mechanism of the cAMP-dependent protein kinase catalytic subunit from porcine heart as deduced from the 2.0 Å structure of the complex with manganese(2+) adenylyl imidodiphosphate and inhibitor peptide PKI(5–24), *EMBO J.* **12**, 849–859.
44. Larsen, T. M., Benning, M. M., Rayment, I., and Reed, G. H. (1998) Structure of the Bis(Mg²⁺)-ATP-oxalate complex of the rabbit muscle pyruvate kinase at 2.1 Å resolution: ATP binding over a barrel, *Biochemistry* **37**, 6247–6255.

BI0495073